Structural Probing of a Microdomain in the Dopamine Transporter by Engineering of Artificial Zn^{2+} Binding Sites†

Lene Norregaard,‡,§ Irache Visiers,|| Claus J. Loland,‡ Juan Ballesteros,|| Harel Weinstein,|| and Ulrik Gether*,‡

Division of Cellular and Molecular Physiology, Department of Medical Physiology, Panum Institute, University of Copenhagen, DK-2200 Copenhagen N, Denmark, Department of Neurochemistry, NeuroSearch A/S, Ballerup, Denmark, and Department of Physiology and Biophysics, Mount Sinai School of Medicine, New York, New York 10029

Received August 3, 2000; Revised Manuscript Received October 24, 2000

ABSTRACT: Previously, we have identified three Zn^{2+} binding residues in an endogenous Zn^{2+} binding site in the human dopamine transporter (hDAT): ^{193}His in extracellular loop 2 (ECL 2), ^{375}His at the external end of transmembrane segment (TM) 7, and ^{396}Glu at the external end of TM 8. Here we have generated a series of artificial Zn^{2+} binding sites in a domain situated around the external ends of TMs 7 and 8 by taking advantage of the well-defined structural constraints for binding of the zinc(II) ion. Initially, we found that the Zn^{2+}-coordinating ^{193}His in ECL 2 could be substituted with a histidine inserted at the $i - 4$ position relative to ^{375}His in TM 7. In this mutant (H193K/M371H), Zn^{2+} potently inhibited [^{3}H]dopamine uptake with an IC_{50} value of 7 μM as compared to a value of 300 μM for the control (H193K). These data are consistent with the presence of an α-helical configuration of TM 7. This inference was further corroborated by the observation that no increase in the apparent Zn^{2+} affinity was observed following introduction of histidines at the $i - 2$, $i - 3$, and $i - 5$ positions. In contrast, introduction of histidines at positions $i + 2$, $i + 3$, and $i + 4$ all resulted in potent inhibition of [^{3}H]dopamine uptake by Zn^{2+} ($IC_{50} = 3-32$ μM). These observations are inconsistent with continuation of the helix beyond position 375 and indicate an approximate boundary between the end of the helix and the succeeding loop. In summary, the data presented here provide new insight into the structure of a functionally important domain in the hDAT and illustrate how engineering of Zn^{2+} binding sites can be a useful approach for probing both secondary and tertiary structure relationships in membrane proteins of unknown structure.

The dopamine transporter (DAT)[1] belongs, together with the closely related norepinephrine (NET) and serotonin (SERT) transporters, to a family of Na^+/Cl^--dependent solute carriers that are characterized functionally by coupling translocation of substrate with cotransport of Na^+ and Cl^- (*1*, *2*). By mediating rapid reuptake of released dopamine into the presynaptic nerve terminal, the DAT controls the amount of available dopamine in the synaptic cleft (*3*, *4*). In this way, the DAT plays a key role in regulation of dopaminergic neurotransmission (*3*, *4*). Of significant interest, the DAT is a target for commonly abused psychostimulants, such as cocaine and amphetamine, which are able to block reuptake of dopamine via the DAT (*2*−*4*). Although cocaine and amphetamine also inhibit the function of SERT and NET, there is substantial evidence indicating that inhibition of the DAT is a predominant mechanism underlying the stimulatory effects of these drugs (*5*−*7*).

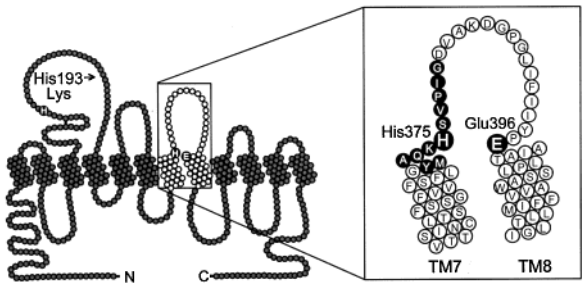

FIGURE 1: Two-dimensional representation of the human dopamine transporter (hDAT). The three residues that were identified previously as coordinates in an endogenous Zn^{2+} binding site of hDAT (^{193}His, ^{375}His, and ^{396}Glu) (*12*, *13*) are shown (white letters in enlarged black circles). To generate new artificial Zn^{2+} binding sites at the external end of TM 7 and TM 8 (enlarged region), Zn^{2+}-coordinating ^{193}His was mutated to lysine, which is present in the corresponding position in the hNET. The positions indicated with white letters in small black circles were mutated to histidines as described in the text.

All Na^+/Cl^--dependent carriers are believed to share a common topology characterized by the presence of 12 transmembrane segments connected by alternating extracellular and intracellular loops with an intracellular location of the N- and C-terminus (Figure 1) (*1*, *2*, *4*). Importantly, this topology has been supported by several recent studies

† The study was supported by the Danish Natural Science Research Council, the Carlsberg Foundation, the NOVO Nordisk Foundation, and National Institutes of Health Grant P01 DA 12408.

* To whom correspondence should be addressed: Division of Cellular and Molecular Physiology, Department of Medical Physiology 12-5-22, Panum Institute, University of Copenhagen, DK-2200 Copenhagen N, Denmark. Telephone: +45 3532 7548. Fax: +45 3532 7555. E-mail: gether@mfi.ku.dk.

‡ University of Copenhagen.

§ NeuroSearch A/S.

|| Mount Sinai School of Medicine.

[1] Abbreviations: DAT, dopamine transporter; NET, norepinephrine transporter; SERT, serotonin transporter; hDAT, human dopamine transporter; TM, transmembrane segment; ECL, extracellular loop; WT, wild-type; HdP, mean hydrophobicity; SE, standard error.

10.1021/bi0018335 CCC: $19.00
Published on Web 11/30/2000

(*8*−*13*). A distinctive feature of the Na^+/Cl^--dependent carriers is a large 70−80-amino acid extracellular loop connecting the third and fourth transmembrane segment (*1*, *2*, *4*). The loop contains consensus sites for N-linked glycosylation and two entirely conserved cysteines presumed to form a disulfide bridge (*1*, *2*, *4*). Many studies have been carried out in an attempt to define functional domains in Na^+/Cl^--dependent carriers. The application of a variety of mutagenesis-based approaches, such as construction of chimeric transporters (*14*−*17*), point mutational analysis (*18*−*21*), random mutagenesis (*22*), and the substituted cysteine accessibility method (*11*, *23*), has provided information about domains and residues involved in the transport process or binding of the substrate and/or blockers. Nevertheless, only very limited insight has accrued so far concerning the secondary and tertiary structure of this class of transporters. Recently, we have been able to describe the first distance constraints in the tertiary structure of the human DAT (hDAT) based on the discovery of an endogenous high-affinity Zn^{2+} binding site (*12*, *13*). Initially, we observed that Zn^{2+}, at micromolar physiological concentrations, acts as a potent noncompetitive blocker of dopamine uptake (*12*). Furthermore, we found that micromolar concentrations of Zn^{2+} markedly potentiate binding of the cocaine-like blocker, WIN 35,428 (*12*). Systematic mutation of potential Zn^{2+} binding residues, predicted to be on the extracellular face of the transporter, identified three residues as three coordinating ligands in this endogenous Zn^{2+} binding site (*12*, *13*) (Figure 1): ^{193}His in the second extracellular loop, ^{375}His at the external end of the putative transmembrane segment (TM) 7, and ^{396}Glu at the external end of TM 8. The three residues are distant in the primary structure, but their common participation in binding of the small zinc(II) ion defined their spatial proximity in the tertiary structure of the transporter (*12*, *13*).

The ability of Zn^{2+} to inhibit the translocation process by coordinating residues situated spatially around the external ends of TM 7 and 8 of the hDAT indicated a role of this region in the substrate translocation mechanism. In the study presented here, we probe the structure of this "TM 7/8 microdomain" by taking advantage of the strict geometrical requirements for binding of the zinc(II) ion. The structures of many soluble Zn^{2+} binding proteins are known from X-ray crystallography, and therefore, the geometry of the interactions between Zn^{2+} and the coordinating residues is well-characterized (*24*−*26*). Most importantly, we find that if two coordinating histidine residues are localized within the same α-helix, the histidines are, according to known structures of naturally occurring Zn^{2+} binding sites, separated by three residues (*i* and $i + 4$ or $i - 4$) (Figure 2A). In contrast, if the two coordinating histidine residues are localized within a *β*-strand, they are separated by only one residue (*i* and $i + 2$ or $i - 2$) (Figure 2B). On the basis of this information, we have generated a series of new Zn^{2+} binding sites by performing systematic histidine substitutions corresponding to the outer portion of TM 7 in the hDAT. In addition to describing the relative orientation between TM 7 and TM 8, the results support the presence of an α-helical configuration of the outer portion of the predicted TM 7 and define an approximate boundary between the end of the helix and the succeeding loop region. Furthermore, this information, together with data from our previous studies, enables us to build a structural model of the TM 7/8 microdomain. This model incorporates the structural constraints from known Zn^{2+} binding sites, and refines the analysis and predictions of structural features in a functionally important region of the hDAT.

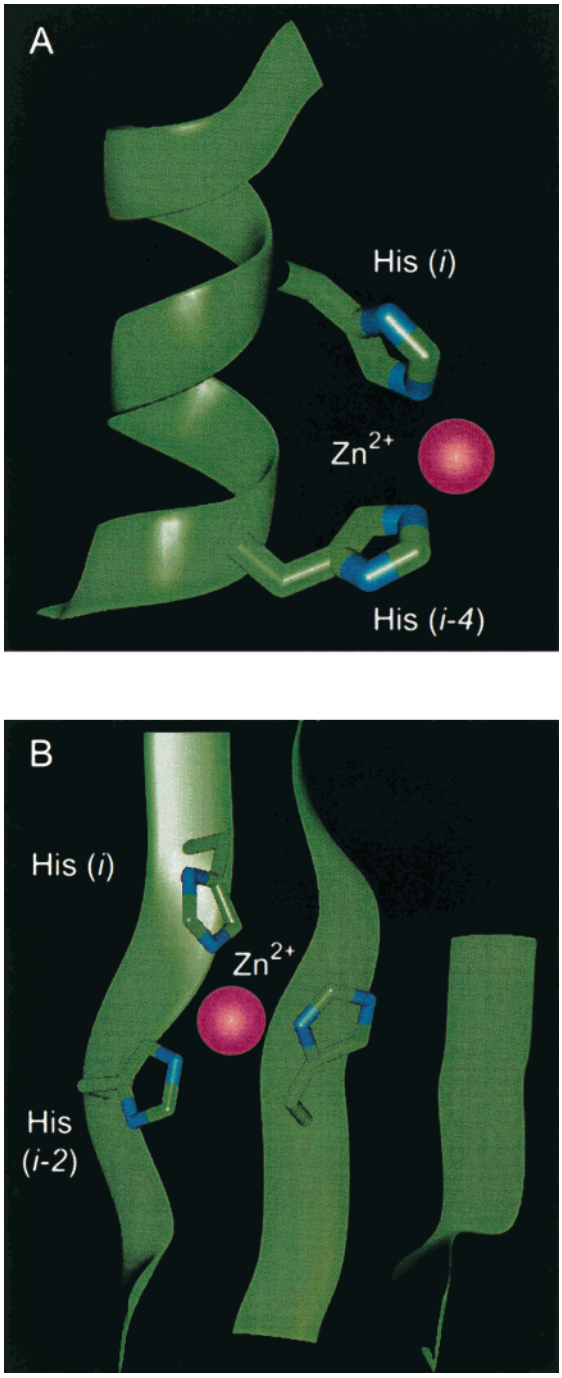

FIGURE 2: Structural constraints for binding of Zn^{2+} between two histidine residues in an α-helix or *β*-strand. (A) Coordination of Zn^{2+} between two histidines present in an α-helix requires that the two histidines are positioned as *i* and $i - 4$ with *i* assuming the gauche+ rotamer and $i - 4$ the trans rotamer. The figure shows ^{140}His and ^{144}His in the endogenous Zn^{2+} binding site of the elastase of *Pseudomonas aeruginosa* (1.5 Å resolution) (*50*). (B) Coordination of Zn^{2+} between two histidines present in a *β*-strand requires that the two histidines are positioned as *i* and $i - 2$ with *i* assuming the gauche+ rotamer and $i - 2$ the trans rotamer. The figure shows ^{94}His and ^{96}His in the endogenous Zn^{2+} binding site of carbonic anhydrase II (1.54 Å resolution) (*51*). The histidine in the adjacent strand (^{119}His) forms the third coordinate in the binding site.

EXPERIMENTAL PROCEDURES

Site-Directed Mutagenesis. The cDNA encoding the hDAT was kindly provided by M. G. Caron (Duke University, Durham, NC). The mutant transporters were constructed by PCR-derived mutagenesis using *Pfu* polymerase according to the manufacturer's instructions (Stratagene, La Jolla, CA). The generated PCR fragments were digested with the appropriate enzymes, purified by agarose gel electrophoresis, and cloned into the eukaryotic expression vector, pRC/CMV, containing hDAT (*15*, *27*). All mutations were confirmed by restriction enzyme mapping and DNA sequencing using an ABI 310 automated sequencer.

Cell Culture and Transfection. COS-7 cells were grown in Dulbecco's modified Eagle's medium (DMEM) 041 31885 supplemented with 10% fetal calf serum, 2 mM L-glutamine, and 0.01 mg/mL gentamicin. Wild-type and mutant constructs in pRC/CMV were transiently transfected into COS-7 cells by the calcium phosphate precipitation method as previously described (*28*, *29*).

[^{3}H]Dopamine Uptake Experiments. Uptake assays were modified from Giros et al. (*30*) using 2,5,6-[^{3}H]dopamine (6−21 Ci/mmol) (Amersham, Little Chalfont, U.K.). Transfected COS-7 cells were plated in either 24-well dishes (10^5 cells/well) or 12-well dishes ($2-3 \times 10^5$ cells/well) to achieve an uptake level of 5−10% of the total amount of added [^{3}H]dopamine. The uptake assays were carried out 2 days after transfection. Prior to the experiment, the cells were washed once in 500 μL of uptake buffer [25 mM HEPES (pH 7.4) containing 130 mM NaCl, 5.4 mM KCl, 1.2 mM $CaCl_2$, 1.2 mM $MgSO_4$, 1 mM L-ascorbic acid, and 5 mM D-glucose (pH 7.4)]. Nonlabeled compounds were added to the cells at the indicated concentrations together with 20 nM [^{3}H]dopamine in a final volume of 250 μL (24-well dishes) or 500 μL (12-well dishes). After incubation for 10 min at 37 °C, the cells were washed twice with 500 μL of uptake buffer, lysed in 250 μL (24-well dishes) or 300 μL (12-well dishes) of 1% sodium dodecyl sulfate (SDS), and left for 1 h at 37 °C. All samples were transferred to 24-well counting plates (Wallac, Turku, Finland) followed by addition of 500 μL (24-well dishes) or 600 μL (12-well dishes) of Opti-phase Hi Safe 3 scintillation fluid (Wallac) and subsequent counting of the plates in a Wallac Tri-Lux β scintillation counter (Wallac). The level of nonspecific uptake was determined in the presence of 1 mM nonlabeled dopamine (RBI, Natick, MA). All determinations were performed in triplicate.

Ligand Binding. Binding assays were carried out on whole cells using [^{125}I]RTI-55 (2200 Ci/mmol) (Dupont-NEN, Boston, MA) as the radioligand. Twenty-four hours after transfection, cells were seeded in 24-well dishes (10^4-10^5 cells/well) to achieve a binding level of 5−10% of the total amount of added [^{125}I]RTI-55. Two days after transfection, competition binding assays were performed in a final volume of 250 μL of uptake buffer containing 0.2 nM [^{125}I]RTI-55 and the following concentrations of RTI-55 (0, 10^{-11}, 10^{-10}, 3×10^{-10}, 10^{-9}, 3×10^{-9}, 10^{-8}, 3×10^{-8}, 3×10^{-7}, 10^{-7}, 10^{-6}, and 10^{-5} M) or Zn^{2+} (0, 10^{-8}, 10^{-7}, 3×10^{-7}, 10^{-6}, 2×10^{-6}, 5×10^{-6}, 10^{-5}, 3×10^{-4}, 10^{-4}, 3×10^{-4}, and 10^{-3} M). Binding was terminated after 2 h at 4 °C by washing the cells twice in 500 μL of uptake buffer prior to lysis in 250 μL of 1% sodium dodecyl sulfate for 1 h at 37 °C. All samples were transferred to 24-well counting plates, followed by addition of 500 μL of Opti-phase Hi Safe 3 scintillation fluid (Wallac) and subsequent counting of the plates in a Wallac Tri-Lux β scintillation counter (Wallac). The level of nonspecific binding was determined in the presence of 10 μM RTI-55. Determinations were made in triplicate.

Calculations. Uptake and binding data were analyzed by nonlinear regression analysis using Prism 2.0 from GraphPad Software (San Diego, CA).

Computational Methods. *(1) Multiple-Sequence Alignment.* The secondary structure assignment was based on a multiple-sequence alignment analysis (MSAA) of conservation and physicochemical properties as described previously (*31*), following protocols that have yielded structural information for a variety of transmembrane proteins (*32*−*38*). For the hydrophobicity analysis, the sequence alignment is scanned with a window of seven residues and the mean hydrophobicity (HdP) is calculated for each window using the Kyte−Doolitle scale (*39*). For the analysis of sequence conservation, the criteria evaluate both the conservation at the site and the relations among the amino acid substituents with the use of a mutation matrix (*40*).

(2) Molecular Modeling. In the molecular models, the helical portions were built as ideal α-helices. All of the Zn^{2+} binding sites were modeled assuming a tetrahedral geometry. The choice of tautomeric forms of the Zn^{2+}-bound histidines [i.e., the NE2 (ϵ tautomer) vs ND1 (δ tautomer)] was based on statistical observations from crystal structures of Zn^{2+}-containing proteins in which 70% of the Zn^{2+}-bound histidines are ϵ tautomers (*26*). Distances and angles between coordinating atoms and the Zn^{2+} were obtained from the literature (*26*) and used in the modeling process. Three Zn^{2+} binding sites were modeled, the endogenous Zn^{2+} site in hDAT (^{193}His-^{375}His-^{396}Glu) and two engineered Zn^{2+} sites (^{375}His-^{400}Cys and ^{371}His-^{375}His-^{396}Glu). The structural criteria and constraints were applied uniformly to be satisfied by all models. The relative orientation of the two helical fragments corresponding to the outer portion of TM 7 (residues ^{371}Met−^{375}His) and the outer portion of TM 8 (residues ^{396}Glu−^{400}Thr) determines a structure representing the endogenous binding site (^{193}His-^{375}His-^{396}Glu). Since this site has only one coordinating residue in each helix, the initial relative orientation of TM 7 and the TM 8 fragments was arbitrarily selected among the combinations that can achieve a Zn^{2+}-coordinating geometry. A series of cycles of manual refinement produced a final structure that was compatible with the experimentally derived Zn^{2+} binding sites, satisfied up to sterically allowed changes in the side chain dihedral angles of the residues involved (but without variation of the relative backbone orientation of the two fragments). The first cycle of refinement involved the constraints imposed by modeling the ^{375}His-^{400}Cys binding site generated by removal of ^{193}His and mutation of ^{400}Thr to Cys. Manual rigid body movements as well as side chain rotations were performed until a structure was achieved that satisfied the requirement for this new Zn^{2+} binding site. As the initial set of distances between the coordinating atoms and the zinc(II) ion was lost in this manipulation, the subsequent modeling cycle was used to recover the binding of the original site. The two cycles were iterated until a structure was obtained in which the two Zn^{2+} binding sites differ only by side chain rotations. On the basis of the structure that satisfies both the endogenous

site and the ^{375}His-^{400}Cys Zn^{2+} site, the modeling cycles were repeated for the third binding site (^{371}His-^{375}His-^{396}Glu), until a final structure was obtained that satisfies all three binding sites through side chain rotations alone, without a change in the backbone orientation of the helices. All molecular modeling procedures were performed on a SGI O2 workstation using the Insight II software package (Molecular Simulations, San Diego, CA).

RESULTS

Structural Constraints for Zn^{2+} Binding. Comprehensive database searches of known structures of naturally occurring Zn^{2+} binding sites have corroborated the strict structural constraints for coordination of the zinc(II) ion (*26*). For the majority of sites, a tetrahedral coordination geometry is observed involving the side chains of four residues or the side chains of three residues in addition to a water molecule (*26*). The Zn^{2+}-coordinating side chains are almost exclusively the imidazole side chain of histidines, the sulfhydryl side chain of cysteines, and the carboxylate side chains of glutamates and aspartates. Remarkably well-defined structural constraints were observed when two Zn^{2+}-coordinating histidines were located in the same α-helix or β-strand. As illustrated in Figure 2A, coordination of Zn^{2+} between two histidines located in an α-helix requires that the two histidines be positioned as i and $i - 4$ with i assuming the gauche+ rotamer and $i - 4$ the trans rotamer. Importantly, if the two residues are positioned as either i and $i - 3$ or i and $i - 5$, binding of Zn^{2+} will involve a substantial distortion of the helix (not shown). A similar strict pattern was observed for pairs of Zn^{2+}-binding histidines in β-strands. Two histidines within a β-strand must be positioned as i and $i - 2$ to bind Zn^{2+} without distortion of the strand (Figure 2B). These observations suggested the possibility that Zn^{2+} binding sites engineered by inserting pairs of histidines in selected protein segments could prove to be a useful tool for probing secondary structure relationships in a protein of unknown structure such as the hDAT.

Sequence Analysis of TM 7 in the hDAT. A hydrophobicity analysis of the predicted TM 7 in Na^+/Cl^--dependent transporters is shown in Figure 3A. The mean hydrophobicity (HdP), determined as described in Experimental Procedures, is plotted against the amino acid sequence of TM 7 in the hDAT. This plot identifies the putative TM 7 segment from position 346 to 372 as a continuous stretch with high overall hydrophobicity and an approximate periodicity of three or four residues, which is consistent with an α-helical configuration. Next, we analyzed the conservation pattern of Na^+/Cl^--dependent transporters in the TM 7 segment and plotted it against the amino acid sequence of hDAT (Figure 3B). The conservation periodicity pattern can be divided into three main regions. Region I, comprising residues ^{351}Ser−^{362}Phe, displays a periodicity of three or four residues, again indicative of a possible helical configuration, where the conserved face coincides with the polar one identified from the hydrophobicity plot. Region II includes residues ^{360}Ser−^{372}Ala and represents an almost continuos fragment of 12 highly conserved residues. Region III includes six sequentially nonconserved residues (^{373}Gln−^{378}Pro) (Figure 3B), five of which correspond to mostly hydrophilic positions (Figure 3A). The change in both the conservation pattern and hydrophobicity pattern would predict that the end of TM 7 would be around position 372. As described below, we decided to explore these theoretical predictions experimentally by taking advantage of the strict structural requirements for binding of the zinc(II) ion.

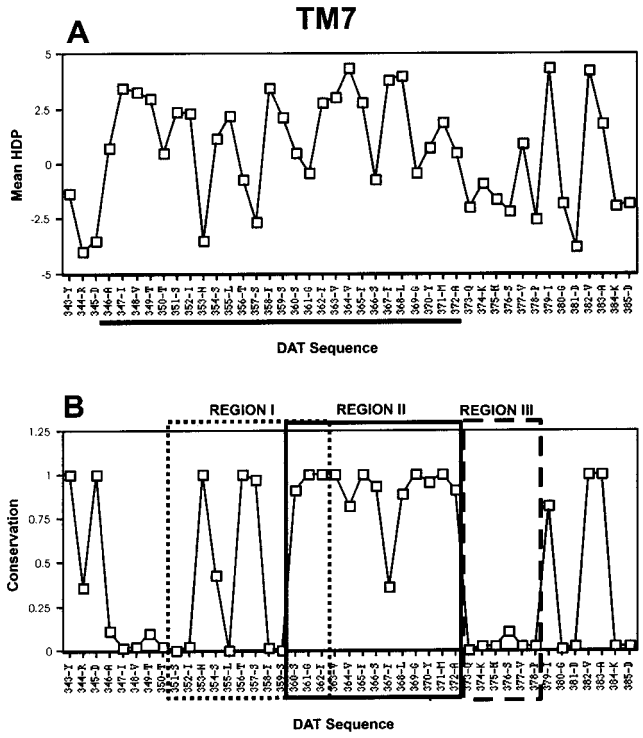

FIGURE 3: Sequence analysis of TM 7 in the hDAT. (A) Hydrophobicity analysis of TM 7 in Na^+/Cl^--dependent transporters with mean hydrophobicity (HDP) plotted against the amino acid sequence of the hDAT. (B) Sequence conservation pattern in TM 7 Na^+/Cl^--dependent transporters plotted against the amino acid sequence in the hDAT. For the analysis of sequence conservation, the criteria evaluate both the conservation at the site and the relations among the amino acid substituents with the use of a mutation matrix (*40*). The conservation periodicity pattern can be divided into three main regions. Region I, comprising residues ^{351}Ser−^{362}Phe, displays a periodicity of three or four residues, again indicative of a possible helical configuration, where the conserved face coincides with the polar one identified from the hydrophobicity plot. Region II includes residues ^{360}Ser−^{372}Ala and represents an almost continuous fragment of 12 highly conserved residues. Region III includes six sequentially nonconserved residues (^{373}Gln−^{378}Pro) (B), five of which correspond to mostly hydrophilic positions (A).

Construction of a Zn^{2+} Binding Site at the External End of TM 7 in the hDAT Containing Two Intrahelical Histidines. Zn^{2+} is a potent noncompetitive inhibitor of [^{3}H]dopamine uptake in COS-7 cells transiently expressing the hDAT (Figure 4 and Table 1) (*12*). The Zn^{2+} inhibition curve is biphasic with an IC_{50} for the high-affinity phase of 0.47 μM (Table 1 and Figure 4) (*12*). Previously, we have shown that the high-affinity inhibition occurs via binding of Zn^{2+} to an endogenous Zn^{2+} binding site consisting of three residues of the transporter: ^{193}His in ECL 2, ^{375}His at the external end of TM 7, and ^{396}Glu at the external end of TM 8 (Figure 1) (*12*, *13*). Zn^{2+}-induced inhibition of [^{3}H]dopamine uptake is dependent on the presence of all three residues; hence, mutation of any of the three residues causes a 500−1000-fold increase in the IC_{50} value for Zn^{2+} inhibition of [^{3}H]-dopamine uptake (*12*, *13*).

According to the hydrophobicity plot and conservation pattern outlined in the previous section, ^{375}His is situated

Table 1: Uptake Characteristics for the hDAT and Mutant Transporters[a]

hDAT mutant	$IC_{50}(Zn^{2+})$ (μM) (SE interval)	K_M(dopamine) (μM) (SE interval)	V_{max} [pmol min^{-1} (10^5 cells)$^{-1}$] (means ± SE)	*n*
WT hDAT	0.47 (0.41−0.54)	3.0 (2.7−3.5)	8.1 ± 1	8
H193K (control)	300 (270−340)	2.4 (2.2−2.6)	7 ± 2	4
H193K/M371H	7.0 (6.1−8.1)	1.9 (1.5−2.3)	2.4 ± 1.5	5
H193K/M371H/H375A	720 (610−850)	2 (1.6−2.9)	0.37 ± 0.02	3
H193K/M371H/E396Q	610 (410−910)	2.1 (1.6−2.8)	0.19 ± 0.04	3
H193K/I379H	3.7 (3.1−4.3)	2.4 (1.7−3.3)	0.7 ± 0.3	4
H193K/I379H/H375A	ND	ND	ND	3
H193K/I379H/E396Q	180 (130−270)	1.6 (1.4−1.8)	0.10 ± 0.02	3
H193K/H375A (control)	1040 (750−1450)	5.5 (4.8−6.6)	9 ± 3	3
H193K/G369H/Q373H/H375A	ND	ND	ND	2
H193K/Y370H/K374H/H375A	650 (540−790)	4.7 (4.6−4.8)	0.8 ± 0.3	3
H193K/A372H/S376H/H375A	100 (81−120)	2.0 (1.6−2.6)	0.4 ± 0.2	4
H193K/A372H/S376H/H375A/E396Q	ND	ND	ND	2
H193K/Q373H/V377H/H375A	300 (240−390)	1.6 (1.3−1.9)	0.23 ± 0.07	4
H193K/K374H/P378H/H375A	ND	ND	ND	2

[a] The K_M values for [^{3}H]dopamine uptake were calculated from nonlinear regression analysis of uptake data. Data for Zn^{2+} inhibition of [^{3}H]dopamine uptake were fitted to either a two-site or a one-site model. When fitted to a two-site model, the indicated IC_{50} value for Zn^{2+} is for the high-affinity binding site. The K_M and IC_{50} values are calculated from means of pK_M and pIC_{50}, respectively, and the SE interval from the pK_M and pIC_{50}. ND, not detectable.

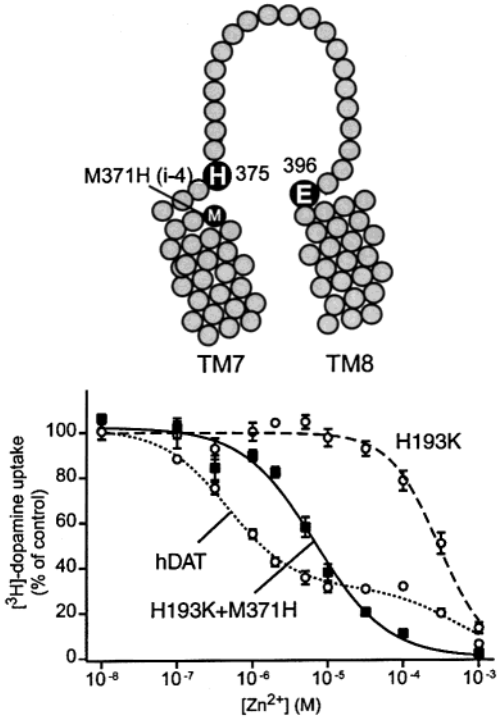

FIGURE 4: Evidence for a Zn^{2+} binding site between ^{371}His, ^{375}His, and ^{396}Glu. (Top) Diagram of TM 7, TM 8, and the connecting loop (ECL 4) with an indication of the Zn^{2+}-coordinating residues. (Bottom) Zn^{2+} inhibition of [^{3}H]dopamine uptake in COS-7 cells transiently expressing the WT hDAT (···), hDAT-H193K (− − −), and hDAT-H193K/M371H (■). Data are means ± the standard error of eight (hDAT), four (hDAT-H193K), and five (hDAT-H193K/M371H) measurements. All experiments were performed in triplicate.

close to the extracellular end of TM 7 (Figure 3). If the transmembrane domain forms an α-helix and if this helix includes ^{375}His, it would be expected that a new Zn^{2+} binding site could be constructed by removing ^{193}His from the endogenous site and substituting this coordinating residue with a histidine at the $i - 4$ position from ^{375}His. As shown in Figure 4, this was in fact possible (Figure 4). Substitution of the methionine at position 371 with a histidine, following removal of ^{193}His (hDAT-H193K/M371H), resulted in potent inhibition of [^{3}H]dopamine uptake by Zn^{2+} ($IC_{50} = 7$ μM), as compared to the control, hDAT-H193K ($IC_{50} = 300$ μM) (Figure 4 and Table 1). Notably, the inhibition curve was monophasic in contrast to the biphasic curve observed for the wild-type (WT) hDAT (Figure 4). Mutation of ^{375}His and ^{396}Glu in hDAT-H193K/M371H increased the IC_{50} values for Zn^{2+} to 720 μM (hDAT-H193K/M371H/H375A) and 610 μM (hDAT-H193K/M371H/E396Q), respectively. This suggests strongly the involvement of these two residues in Zn^{2+} binding to hDAT-H193K/M371H (Table 1). According to Figure 2, these data are consistent with an α-helical configuration at the external end of TM 7 and but inconsistent with the presence of a β-strand.

"Bis-His Scanning" at the External End of TM 7. Next, we sought to define more precisely the structural requirements for binding of Zn^{2+} between a pair of histidines, positioned as i and $i - 4$ at the external end of TM 7, and ^{396}Glu in TM 8. This should further probe the presence of an α-helical configuration at the external end of TM 7, as well as define the orientation of TM 7 relative to TM 8. Accordingly, two histidines, positioned as i and $i - 4$, were "moved around" the hypothetical helical structure (Figure 5). The resulting mutant transporters were functional and demonstrated unchanged K_M values for [^{3}H]dopamine uptake, except for positions 369 and 373 (hDAT-H193K/H375A/G369H/Q373H) and positions 374 and 378 (hDAT-H193K/H375A/K374H/P378H), which were nonfunctional (Table 1). Only insertion of a histidine at the $i + 4$ position from ^{375}His (hDAT-H193K/I379H, named 'I379H' in Figure 5) displayed evidence for high-affinity Zn^{2+} binding (Figure 5 and Table 1). The curve was biphasic with an IC_{50} value of 3.7 μM for the high-affinity phase (Figure 5 and Table 1). Mutation of ^{396}Glu in this construct (hDAT-H193K/I379H/E396Q) eliminated the high-affinity phase, indicating that this residue participates in Zn^{2+} binding to hDAT-H193K/I379H (Table 1). Unfortunately, mutation of ^{375}His (hDAT-H193K/H375A/I379H) resulted in a nonfunctional transporter, so the likely involvement of ^{375}His could not be assessed directly (Table 1). Neither insertion of histidines

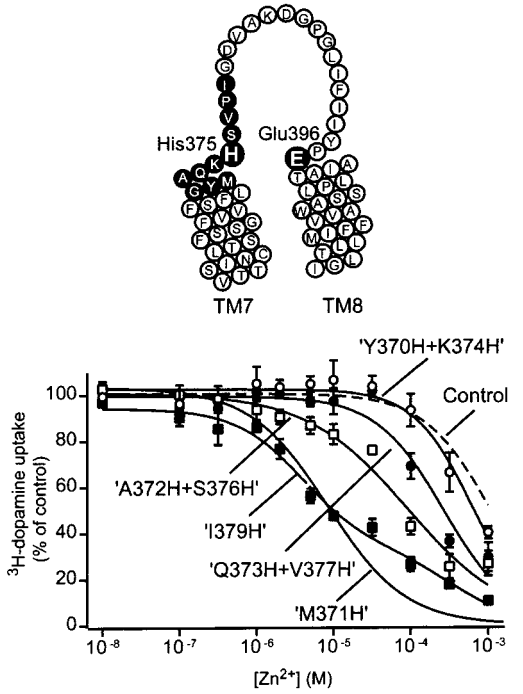

FIGURE 5: Bis-His scanning in the external part of TM 7. (Top) Diagram of TM 7, TM 8, and the connecting loop (ECL 4) with an indication of the residues that are mutated. (Bottom) Zn^{2+} inhibition of [^{3}H]dopamine uptake in COS-7 cells transiently expressing hDAT-H193K/H375A/Y370H/K374H ['Y370H+K374H' (○)], hDAT-H193K/H375A/A372H/S376H ['A372H+S376H' (□)], hDAT-H193K/H375A/Q373H/V377H ['Q373H+V377H' (●)], hDAT-H193K/I379H ['I379H' (■)], hDAT-H193K/M371H ['M371H' (—)], and hDAT-H193K/H375A (— — —). Data are means ± the standard error of three to five measurements. All experiments were performed in triplicate.

at positions 370 and 374 (hDAT-H193K/H375A/Y370H/K374H, named 'Y370H+K374H' in Figure 5) nor insertion at positions 373 and 377 (hDAT-H193K/H375A/Q373H/V377H, named 'Q373H+V377H' in Figure 5) resulted in apparent high-affinity Zn^{2+} binding, i.e., apparent affinities in the sub-micromolar to low micromolar range that should normally be expected for Zn^{2+} binding sites involving three coordinating residues (*41*−*43*) (Table 1). For positions 372 and 376 (hDAT-H193K/H375A/A372H/S376H, named 'A372H+S376H' in Figure 5), we observed an IC_{50} value of 100 μM for Zn^{2+} inhibition of [^{3}H]dopamine uptake representing a nearly 10-fold increase in the apparent Zn^{2+} affinity as compared to the control (hDAT-H193K/H375A). It is possible that the histidines inserted at positions 372 and 376 are capable of coordinating Zn^{2+} together with ^{396}Glu; however, the low affinity suggests an unfavorable geometry of this putative Zn^{2+} binding site.

Evidence for an α-Helical Configuration from Position 371 to 375 and a Loop Configuration between Positions 375 and 379. The data presented so far could support an α-helical configuration in the entire segment from position 371 to 379, at least in the Zn^{2+}-bound state. If the entire segment were helical, the structural constraints for binding of Zn^{2+} to pairs of histidines in α-helices would predict no increase or only minor increases in Zn^{2+} affinities from introducing histidines at either the $i \pm 2$, $i \pm 3$, or $i \pm 5$ positions relative to ^{375}His in the hDAT-H193K background (Figure 6). However, if the segment from position 371 to 379 is not α-helical but forms a flexible structure, it could be expected that Zn^{2+}

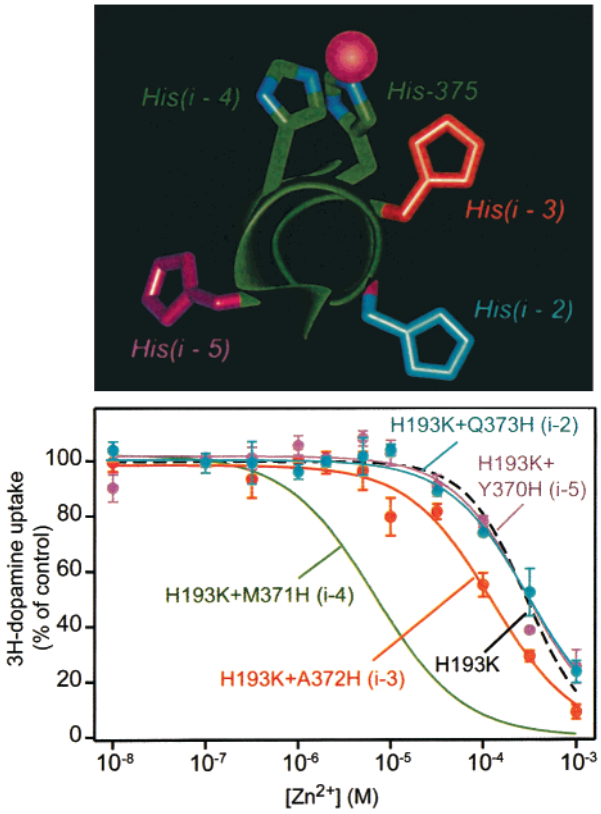

FIGURE 6: Evidence for an α-helical conformation between positions 371 and 375 of the hDAT. (Top) Differences between histidines positioned at $i - 2$, $i - 3$, $i - 4$, or $i - 5$ in their proximity to histidine *i*. The structure shown is the same as in Figure 2A with the illustration of His (*i*)−Zn^{2+}−His ($i - 4$) coordination; however, in this figure, the helix is shown down its axis. A histidine has been added corresponding to $i - 2$ (blue), $i - 3$ (red), and $i - 5$ (purple), illustrating that $i - 4$ is best positioned to coordinate Zn^{2+} together with *i*. By analyzing alternative conformations of all histidines, we found that $i - 3$ may be able to coordinate Zn^{2+}, but that it will require a significant distortion in the conformation of the histidine side chains in an α-helix and thus significantly more energy than $i - 4$. Coordination by histidine at $i - 5$ or $i - 2$ would require gross distortion of the helical backbone and therefore even more energy than the $i - 3$ case. (Bottom) Zn^{2+} inhibition of [^{3}H]dopamine uptake in COS-7 cells transiently expressing hDAT-H193K/Q373H ($i - 2$) (blue), hDAT-H193K/A372H (red), hDAT-H193K/Y370H (purple), and hDAT-H193K/M371H (solid green line). Data are means ± the standard error of three to five measurements. All experiments were performed in triplicate.

will be able to bind not only between ^{375}His and a histidine introduced at the $i - 4$ position (M371H) or the $i + 4$ position (I379H) but potentially also between ^{375}His and histidines at either the $i \pm 2$, $i \pm 3$, or $i \pm 5$ positions. Consequently, a new series of mutant transporters was constructed (Table 2). As shown in Table 2, this new series of mutant transporters was functional and displayed K_M values for [^{3}H]dopamine uptake similar to that of the WT hDAT.

Consistent with an α-helical configuration between residues 371 and 375, introduction of histidines at either the $i - 5$ position (hDAT-H193K/Y370H), the $i - 3$ position (hDAT-H193K/A372H), or the $i - 2$ position (hDAT-H193K/Q373H) from ^{375}His did not demonstrate evidence for high-affinity Zn^{2+} binding (Figure 6 and Table 2). For the $i - 2$ position (hDAT-H193K/Q373H) and the $i - 5$ position (hDAT-H193K/Y370H), the IC_{50} values for Zn^{2+} were almost identical to the control (hDAT-H193K) (Table

Table 2: Uptake Characteristics for the hDAT and Mutant Transporters[a]

hDAT mutant	$IC_{50}(Zn^{2+})$ (μM) (SE interval)	K_M(dopamine) (μM) (SE interval)	V_{max} [pmol min^{-1} (10^5 cells)$^{-1}$] (means ± SE)	*n*
H193K (control)	300 (270−340)	3.0 (2.7−3.5)	7 ± 2	4
H193K/Y370H (*i* − 5)	360 (320−410)	1.7 (1.4−2.2)	2.6 ± 0.4	4
H193K/M371H (*i* − 4)	7.0 (6.1−8.1)	1.9 (1.5−2.3)	1.4 ± 0.1	5
H193K/A372H (*i* − 3)	120 (110−130)	2.5 (1.9−3.5)	1.4 ± 0.4	5
H193K/Q373H (*i* − 2)	310 (270−360)	2.7 (2.0−3.7)	9.0 ± 0.8	3
H193K/V377H (*i* + 2)	3.6 (2.8−4.6)	3.6 (3.4−3.8)	1.3 ± 0.6	3
H193K/V377H/H375A	410 (290−580)	2.6 (2.3−2.9)	0.4 ± 0.1	3
H193K/V377H/E396Q	57 (36−89)	2.7 (2.5−2.9)	0.34 ± 0.08	3
H193K/P378H (*i* + 3)	32 (27−38)	1.8 (1.1−3.0)	5 ± 1	4
H193K/P378H/H375A	380 (360−410)	2.6 (2.1−3.1)	1.9 ± 0.7	3
H193K/P378H/E396Q	290 (190−450)	4.0 (3.6−4.4)	3 ± 1	3
H193K/I379H (*i* + 4)	3.7 (3.1−4.3)	3.7 (3.1−4.3)	0.7 ± 0.3	4
H193K/G380H (*i* + 5)	180 (150−220)	2.8 (1.8−4.4)	10 ± 3	3

[a] The K_M values for [^{3}H]dopamine uptake were calculated from nonlinear regression analysis of uptake data. Data for Zn^{2+} inhibition of [^{3}H]dopamine uptake were fitted to either a two-site or a one-site model. When fitted to a two-site model, the indicated IC_{50} value for Zn^{2+} is for the high-affinity binding site. The K_M and IC_{50} values are calculated from means of pK_M and pIC_{50}, respectively, and the SE interval from the pK_M and pIC_{50}.

2). For the *i* − 3 position (hDAT-H193K/A372H), a slight, 2−3-fold, decrease in the IC_{50} value for Zn^{2+} was observed as compared to that of hDAT-H193K (Table 2). Notably, this small increase in the apparent Zn^{2+} affinity for hDAT-H193K/A372H (*i* − 3) might still indicate an α-helical configuration. Whereas Zn^{2+} binding between histidines positioned as *i* and *i* − 2 or *i* and *i* − 5 within an α-helix is impossible, Zn^{2+} binding between histidines positioned as *i* and *i* − 3 can be achieved, but only by forcing some distortion of the helix, which would lead to a loss of affinity (Figure 6). Hence, the apparent low-affinity binding of Zn^{2+} to hDAT-H193K/A372H (IC_{50} = 120 μM) could reflect Zn^{2+} binding between ^{375}His and A372H in a distorted helix with the possible additional involvement of ^{396}Glu.

The results for the segment between positions 375 and 379 were very different from those obtained for the segment between positions 371 and 375. As shown in Figure 7, marked increases in the apparent Zn^{2+} affinities were observed by inserting a histidine not only at the *i* + 4 position from ^{375}His (hDAT-H193K/I379H) but also at the *i* + 2 position (hDAT-H193K/V377H) and the *i* + 3 position (hDAT-H193K/P378H). The highest apparent Zn^{2+} affinity was observed for hDAT-H193K/V377H, which displayed an IC_{50} value for Zn^{2+} of 3.6 μM, whereas the IC_{50} was 32 μM for hDAT-H193K/P378H (Table 2). To ensure that Zn^{2+} binding to these two mutants did involve both ^{375}His and ^{396}Glu, these two residues were mutated one by one in hDAT-H193K/V377H and hDAT-H193K/P378H. Mutation of ^{375}His and ^{396}Glu in hDAT-H193K/P378H (hDAT-H193K/H375A/P378H and hDAT-H193K/P378H/E396Q) increased the IC_{50} value for Zn^{2+} 12- and 9-fold, respectively, in full agreement with the involvement of both residues in Zn^{2+} binding (Table 2). Similarly, mutation of ^{375}His in hDAT-H193K/V377H (hDAT-H193K/H375A/V377H) increased the IC_{50} value for Zn^{2+} around 100-fold whereas mutation of ^{396}Glu (hDAT-H193K/V377H/E396Q) increased the IC_{50} value 15-fold, again in full agreement with the involvement of both residues in Zn^{2+} binding (Table 2). Notably, the IC_{50} value of 57 μM for Zn^{2+} in hDAT-H193K/V377H/E396Q suggests the interesting possibility that binding of Zn^{2+} by ^{375}His and a histidine at position 377 is sufficient to promote an inhibition of transport (Table 2). Taken together, the data are inconsistent with an α-helical configuration between residue 375 and residue 379 and strongly suggest the absence of a well-defined secondary structure (neither α-helical nor β-strand).

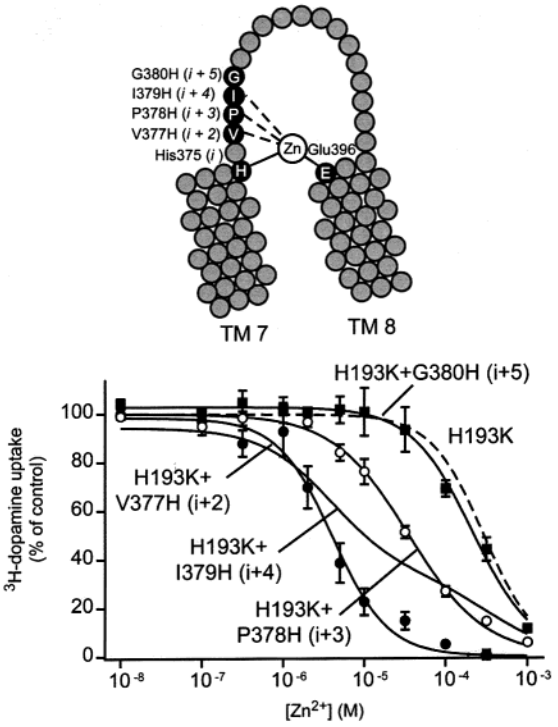

FIGURE 7: Evidence for loop configuration between positions 375 and 379 of the hDAT. (Top) TM 7 and TM 8 with the connecting fourth extracellular loop. Histidines were introduced at the indicated positions in the background of hDAT-H193K. (Bottom) Zn^{2+} inhibition of [^{3}H]dopamine uptake in COS-7 cells transiently expressing hDAT-H193K/V377H (*i* + 2) (●), hDAT-H193K/P378H (*i* + 3) (○), hDAT-H193K/G380H (*i* + 5) (■), hDAT-H193K/I379H (—), and hDAT-H193K (− − −). Data are means ± the standard error of three to five measurements. All experiments were performed in triplicate.

Molecular Mechanism of Zn^{2+} Inhibition. At the wild-type hDAT, Zn^{2+} acts as a noncompetitive inhibitor of [^{3}H]-dopamine uptake; thus, Zn^{2+} decreases the V_{max} for [^{3}H]-dopamine uptake without affecting K_M (*12*). The molecular mechanism of Zn^{2+} inhibition was investigated in three of the mutant transporters containing a Zn^{2+} binding site with an apparent affinity in the micromolar to sub-micromolar

Table 3: Uptake Characteristics for the hDAT and Mutant Transporters[a]

	in the absence of Zn^{2+}		in the presence of Zn^{2+}		
mutant	K_M(dopamine) (μM) (SE interval)	V_{max} (normalized in % for each construct)	K_M(dopamine) (μM) (SE interval)	V_{max} (% of V_{max} in the absence of Zn^{2+})	*n*
WT hDAT	2.9 (2.5−3.4)	100	3.8 (3.2−4.4)	46 ± 7	4
H193K/M371H	4.4 (3.7−5.4)	100	5.0 (4.6−5.4)	41 ± 6	3
H193K/V377H	4.0 (2.9−5.3)	100	3.7 (2.5−5.4)	29 ± 3	3
H193K/I379H	3.4 (2.6−4.3)	100	2.2 (1.6−3.0)	31 ± 4	3

[a] The K_M values for [^{3}H]dopamine uptake were calculated from nonlinear regression analysis of uptake data. The K_M values are calculated from means of pK_M and the SE interval from the pK_M. For all mutants, the K_M values for [^{3}H]dopamine in the presence and absence of Zn^{2+} (10 μM) are not found to be significantly different; $p > 0.05$, via the two-tailed *t* test. The normalized V_{max} values are as follows: WT hDAT, 8 ± 4 pmol min^{-1} (10^5 cells)$^{-1}$; H193K/M371H, 2.4 ± 1.5 pmol min^{-1} (10^5 cells)$^{-1}$; H193K/V377H, 1.3 ± 0.6 pmol min^{-1} (10^5 cells)$^{-1}$; and H193K/I379H, 0.7 ± 0.3 pmol min^{-1} (10^5 cells)$^{-1}$ (means ± SE).

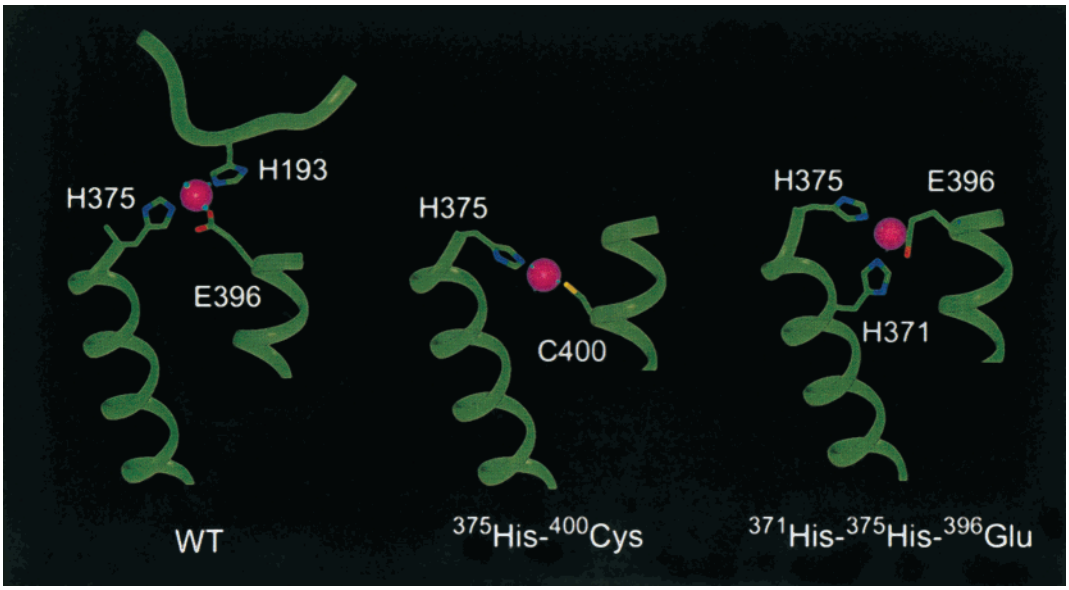

FIGURE 8: Molecular model of the TM 7/8 microdomain. The model incorporates the constraints defined by our data. Three different Zn^{2+} binding sites were included in the modeling procedure. (Left) The endogenous Zn^{2+} binding site in the hDAT (^{193}His-^{375}His-^{396}Glu) (*12*, *13*). (Middle) The engineered site ^{375}His-^{400}Cys described previously (*13*). (Right) The engineered site ^{371}His-^{375}His-^{396}Glu described in this paper. The three Zn^{2+} binding sites were all modeled assuming a tetrahedral coordination geometry. The distances and angles of the three Zn^{2+} binding sites are summarized in Table 4. They are all within the boundaries observed for crystal structures of Zn^{2+}-containing proteins (Table 4). Fragments ^{347}Ile−^{375}His (TM 7) and ^{396}Glu−^{401}Leu (TM 8) were modeled as two ideal antiparallel α-helices with a predicted crossing angle of 161.3° between the axes and a distance between the α-carbon of ^{375}His and ^{396}Glu of 10.4 Å. This relative backbone orientation of TM 7 and TM 8 satisfies all three Zn^{2+} binding sites through side chain rotations alone without changes in the position of the two backbones. Note that the α-helix of TM 8 in the model included only five amino acids as the helical pattern of TM 8 may be be disrupted at position 402 due to the presence of a nonconserved proline (I. Visiers, J. Ballesteros, and H. Weinstein, unpublished observation). This secondary structure assignment is predicted from a multiple-sequence alignment analysis of conservation and physiochemical properties (I. Visiers, J. Ballesteros, and H. Weinstein, unpublished observation) performed as described previously (*31*).

range (hDAT-H193K/M371H, ^{371}His-^{375}His-^{396}Glu; hDAT-H193K/I379H, ^{375}His-^{379}His-^{396}Glu; and hDAT-H193K/V377H, ^{375}His-^{377}His-^{396}Glu). The results of the [^{3}H]-dopamine uptake experiments, carried out in the presence and absence of 10 μM Zn^{2+}, are shown in Table 3. For all three mutants, Zn^{2+} selectively decreased the V_{max} without significant changes in K_M, suggesting a noncompetitive mode of action similar to that observed for the wild-type hDAT (*12*, *13*).

The effects of Zn^{2+} on binding of the cocaine analogue [^{125}I]RTI-55 to the WT hDAT and the three mutant transporters were also investigated. At the WT hDAT, Zn^{2+} caused a potentiation of [^{125}I]RTI-55 binding similar to the potentiation that we have previously reported for binding of [^{3}H]WIN 35,428 (*12*, *13*). However, micromolar concentrations of Zn^{2+} did not cause a potentiation of [^{125}I]RTI-55 binding at the three mutant transporters (hDAT-H193K/M371H, ^{371}His-^{375}His-^{396}Glu; hDAT-H193K/I379H, ^{375}His-^{379}His-^{396}Glu; and hDAT-H193K/V377H, ^{375}His-^{377}His-^{396}Glu) (data not shown). The most likely explanation for the lack of Zn^{2+}-induced potentiation at the mutant transporters is that the potentiation not only is dependent on the interaction between TM 7 and TM 8 but also requires the interaction with ^{193}His in the large third extracellular loop (*12*).

Molecular Modeling. On the basis of the structural constraint defined by the data presented here, together with our previous results (*12*, *13*), we have built a structural model of the TM 7/8 microdomain (Figure 8). As outlined in Experimental Procedures, the model was built using the available information from X-ray crystallography of Zn^{2+} binding proteins. Three different Zn^{2+} binding sites were included in the modeling procedure: the endogenous Zn^{2+} binding site in the hDAT (^{193}His-^{375}His-^{396}Glu) (*12*) and two engineered sites, ^{371}His-^{375}His-^{396}Glu described in this paper and ^{375}His-^{400}Cys described previously (*13*). The distances

Table 4: Distances, Angles, and Dihedral Angles for the Modeled Zn^{2+} Sites

	WT hDAT	^{375}His-^{400}Cys	^{371}His-^{375}His-^{396}Glu	standard values[a]
distances (Å)				
N_{375}−Zn	2.21	2.06	2.05	2.07(0.09) 2.09(0.12)
O_{396}−Zn	2.05	not present	1.98	2.04(0.17) 1.95(0.08)
S_{400}−Zn	not present	1.92	not present	2.21(0.13) 2.35(0.09)
N_{371}−Zn	not present	not present	2.10	2.07(0.09) 2.09(0.12)
angles (deg)				
N_{375}−Zn−N_{193}	116.41	not present	not present	108(6) 112(7)
N_{375}−Zn−O_{396}	116.49	not present	118.75	110(9) 107(12)
N_{375}−Zn−S_{400}	not present	112.86	not present	112(4) 107(7)
N_{375}−Zn−N_{371}	not present	not present	104.84	110(9) 107(12)
N_{371}−Zn−O_{396}	not present	not present	94.22	110(9) 107(12)
χ_1 (deg)				
^{371}His	−	−	−83.45	−
^{375}His	−177.65	−67.75	168	−
^{396}Glu	−68.25	−	−170.8	−
^{400}Cys	−	−61.26	−	−
χ_2 (deg)				
^{371}His	−	−	−48.13	−
^{375}His	−90.67	−6.57	113.28	−
^{396}Glu	−161.36	−	−12.26	−

[a] The standard values designate values observed for Zn^{2+} binding sites in protein crystal structures, and have been taken from Alberts et al. (*26*). Two values are given for each distance and angle. The first one corresponds to catalytic Zn^{2+} sites and the second to structural Zn^{2+} sites. Standard deviations are given in parentheses.

and angles of the three Zn^{2+} binding sites are summarized in Table 4. They are all within the boundaries observed for crystal structures of Zn^{2+}-containing proteins (Table 4). Fragments ^{347}Ile-^{375}His (TM 7) and ^{396}Glu−^{401}Leu (TM 8) were modeled as two ideal antiparallel α-helices with a predicted crossing angle of 161.3° between the axes and a distance between the α-carbon of ^{375}His and ^{396}Glu of 10.4 Å. This relative backbone orientation of TM 7 and TM 8 satisfies all three Zn^{2+} binding sites through side chain rotations alone without changes in the position of the two backbones. The dihedral angles of the residues involved in each of the models are summarized in Table 4. Note that the α-helix of TM 8 in the model included only five amino acids as the helical pattern of TM 8 may be be disrupted at position 402 due to the presence of a nonconserved proline (I. Visiers, J. Ballesteros, and H. Weinstein, unpublished observation). This secondary structure assignment is predicted from a multiple-sequence alignment analysis of conservation and physiochemical properties (I. Visiers, J. Ballesteros, and H. Weinstein, unpublished observation) performed as described previously (*31*). It should also be noted that the ECL 4 loop connecting TM 7 and TM 8 was not included in the model since our data did not support a well-defined structure but rather indicated a significant structural flexibility of the loop.

DISCUSSION

Surprisingly, little is known about the structure of Na^+/Cl^--dependent transporters. It is believed that they possess 12 transmembrane segments connected by alternating extracellular and intracellular loops (Figure 1). However, their actual secondary structure is poorly defined, and the tertiary organization of the putative 12-helix bundle is unknown. In this study, we have probed specific secondary and tertiary structure relations in the hDAT by employing an experimental strategy that utilizes the structural constraints for binding of the zinc(II) ion as a calibration for engineering of artificial Zn^{2+} binding sites. Engineering of artificial metal ion binding sites has previously been used to probe the structure of other membrane proteins, such as the Lac permease of *Escherichia coli* (*44*) and G protein-coupled receptors (*41*, *42*, *45*−*47*). Nevertheless, our study represents a first attempt to use engineering of metal ion binding sites as a more systematic approach to mapping both secondary and tertiary structure relations within a functionally important domain in a membrane protein of unknown structure.

One limitation of our approach is that the assessment of Zn^{2+} binding is based on indirect evidence, i.e., the ability of Zn^{2+} to inhibit transporter function. Unfortunately, direct Zn^{2+} binding measurements using radioactive isotopes of Zn^{2+}, such as ^{65}Zn, cannot be readily accomplished both due to health hazards and due to the relatively low (micromolar) affinity of Zn^{2+}, as compared to the nanomolar affinity required for radioligands in binding assays. Direct assessment of divalent metal ion binding by paramagnetic resonance spectroscopy is also not feasible at present since this will require the availability of relative large quantities of the purified transporter protein (*44*). Since we cannot determine the level of Zn^{2+} binding directly, we are therefore unable to exclude the possibility that Zn^{2+} can bind to some of our constructs without affecting transport function. We would argue, however, that this is not a major problem for the data presented here. For example, potent inhibition of uptake by Zn^{2+} is observed following insertion of a hisitidine at the $i - 4$ position from ^{375}His in the hDAT-H193K background (hDAT-H193K/M371H) (Figure 4). Given this potent inhibition of uptake following insertion of a histidine at the $i - 4$ position, we find it very unlikely that Zn^{2+} is also binding with high affinity to the transporter following insertion of histidines at the $i - 2$, $i - 3$, or $i - 5$ position, but in these cases without inhibiting uptake (Figure 6). Rather, it is more likely that Zn^{2+} is incapable of binding to these mutants with high affinity due to the presence of an α-helical configuration and, thus, that the specificity of the histidine substitutions reflects the actual secondary structure of the protein segment, at least in the Zn^{2+}-bound state. In this context, it should be emphasized that the Zn^{2+}-bound states of the transporter mutants very likely represent conformations of considerable functional relevance. The reduction in V_{max} with no change in K_M following Zn^{2+} binding to ^{371}His-^{375}His-^{396}Glu (hDAT-H193K/M371H), ^{375}His-^{379}His-^{396}Glu (hDAT-H193K/I379H), and ^{375}His-^{377}His-^{396}Glu (hDAT-H193K/V377H) indicates a noncompetitive mechanism where Zn^{2+} selectively blocks the translocation process without affecting dopamine binding to the transporter (Table 3). Furthermore, Zn^{2+} did not affect binding of the cocaine analogue RTI-55 to ^{371}His-^{375}His-^{396}Glu, ^{375}His-^{379}His-^{396}Glu, and ^{375}His-^{377}His-^{396}Glu, again supporting the inference that the transporter is maintained in a functionally relevant state upon Zn^{2+} binding (data not shown).

The data presented here, together with our previous results (*12*, *13*), have provided an important series of conformational constraints in the structure of the hDAT. First, ^{193}His, ^{375}His, and ^{396}Glu were identified as three coordinates in an endogenous Zn^{2+} binding site, thus allowing the conclusion that ^{193}His, ^{375}His, and ^{396}Glu must be in proximity in the tertiary structure of the hDAT (*12*, *13*). Next, we engineered a Zn^{2+} binding site between ^{375}His and a cysteine inserted at position 400 (*13*). In this study, the data from a series of engineered Zn^{2+} binding sites indicate an α-helical configuration corresponding to the outer portion of the predicted TM 7 and suggest an approximate boundary between the C-terminal end of the helix and the beginning of the fourth extracellular loop. Moreover, we could infer the orientation of TM 7 relative to TM 8. A model of the TM 7/8 microdomain that incorporates these structural constraints is shown in Figure 8. This model illustrates how the structural inferences derived from a series of Zn^{2+} binding sites can provide sufficient information for at least an initial structural mapping of a selected protein domain.

Both the hydrophobicity plot of TM 7 and the multiple-sequence alignment analysis predict that the extracellular border of the putative α-helical transmembrane segment is at the level of position 372 (Figure 2). The data presented here show structural evidence that the outer portion of TM 7 is indeed α-helical but also that the helix continues beyond position 372 and includes position 375. A likely explanation for this apparent discrepancy is that the transmembrane helix could continue approximately one turn beyond the surface of the membrane. However, we cannot exclude the alternative possibility that a helical structure for the region between positions 372 and 375 is stabilized preferentially in the Zn^{2+}-bound complex. While the segment must be able to adopt such a conformation in the absence of such stabilization, the binding of Zn^{2+} may reinforce helicity at the external end of TM 7 by stabilizing an otherwise less probable conformation. Whether Zn^{2+} is reinforcing helicity at the external end of TM 7 or the segment containing ^{375}His is stably helical is important when considering the underlying molecular mechanism of noncompetitive Zn^{2+} inhibition of DAT function. If the segment containing ^{375}His is stably helical, it is conceivable that Zn^{2+} exerts its inhibitory function by restraining critical motions of TM 7 relative to TM 8. If instead Zn^{2+} is stabilizing the helicity around ^{375}His, it may exert its action by entailing a conformational change in the connecting extracellular loop (ECL 4), which could play a key role in extracellular gating of the transporter. Support for such a role may be inferred from the significant clustering of conserved and subtype selective residues in the ECL 4 segment, which becomes evident in a sequence alignment (I. Visiers, J. Ballesteros, and H. Weinstein, unpublished observation).

It is clear that further studies are required to clarify the exact molecular mechanism of uptake inhibition upon binding of Zn^{2+} to the engineered binding sites in the TM 7−TM 8 region. For example, it should prove interesting to further probe the structure of the TM 7−TM 8 region by applying, for example, the substituted cysteine accessibility method (*48*). Of interest, an important function of the TM 7−TM 8 region in Na^+/Cl^--dependent neurotransmitter transporters has also been indicated from recent studies in the SERT (*22*, *49*). A random mutagenesis study on TM 7 of the SERT revealed several residues in this transmembrane segment as functionally important by their sensitivity to nonconservative mutations (*22*). These residues were found to cluster on one side of a putative helix, supporting our prediction that TM 7 is adopting an α-helical configuration. Moreover, a role in substrate translocation of the fourth extracellular loop (ECL 4) connecting TM 7 and TM 8 has been suggested on the basis of a series of chimeric transporters in which the extracellular loops of SERT were systematically exchanged with the corresponding domains of the NET (*22*, *49*).

In summary, we have achieved new insight into the structure of a functionally important domain located at the external ends of TM 7 and TM 8 of a Na^+/Cl^--coupled neurotransmitter transporter. In addition to providing new structural information, the ability to engineer several Zn^{2+} binding sites within this domain also defined this region as a potential novel site for ligand-mediated, allosteric modulation of transporter function. In this context, it is interesting to point out that despite the functional consequences of Zn^{2+} binding to this domain, it was found to be distinct from the still unknown binding sites for substrates and cocaine-like blockers in the hDAT, i.e., neither Zn^{2+} nor the mutations themselves affected the binding of dopamine and cocaine-like blockers. It is intriguing to speculate that the structural information acquired in this study might therefore serve in the design of small-molecule compounds that will exert their effect by interacting specifically at this site to modulate transporter function. Thus, structural mapping of functionally important microdomains in transporters, receptors, or ion channels by systematic engineering of artificial Zn^{2+} binding site could prove to be a useful tool in the process of selective drug discovery.

ACKNOWLEDGMENT

Dr. Marc G. Caron is thanked for providing the cDNA encoding the hDAT and Dr. Ivy Carroll for providing the unlabeled RTI-55. Lis Sørensen is thanked for excellent technical assistance. Lars-Ole Gerlach and Søren Rasmussen are thanked for helpful comments on the manuscript. U.G. is the recipient of an Ole Rømer Associate Research Professorship from the Danish Natural Science Research Council.

REFERENCES

1. Giros, B., and Caron, M. G. (1993) *Trends Pharmacol. Sci. 14*, 43−49.
2. Nelson, N. (1998) *J. Neurochem. 71*, 1785−1803.
3. Horn, A. S. (1990) *Prog. Neurobiol. 34*, 387−400.
4. Amara, S. G., and Kuhar, M. J. (1993) *Annu. Rev. Neurosci. 16*, 73−93.
5. Ritz, M. C., Lamb, R. J., Goldberg, S. R., and Kuhar, M. J. (1987) *Science 237*, 1219−1223.
6. Giros, B., Jaber, M., Jones, S. R., Wightman, R. M., and Caron, M. G. (1996) *Nature 379*, 606−612.
7. Wise, R. A. (1996) *Annu. Rev. Neurosci. 19*, 319−340.
8. Bruss, M., Hammermann, R., Brimijoin, S., and Bonisch, H. (1995) *J. Biol. Chem. 270*, 9197−9201.
9. Vaughan, R. A., and Kuhar, M. J. (1996) *J. Biol. Chem. 271*, 21672−21680.
10. Chen, J. G., Liu-Chen, S., and Rudnick, G. (1998) *J. Biol. Chem. 273*, 12675−12681.
11. Ferrer, J., and Javitch, J. A. (1998) *Proc. Natl. Acad. Sci. U.S.A. 95*, 9238−9243.

12. Norregaard, L., Frederiksen, D., Nielsen, E. O., and Gether, U. (1998) *EMBO J. 17*, 4266−4273.
13. Loland, C. J., Norregaard, L., and Gether, U. (1999) *J. Biol. Chem. 274*, 36928−36934.
14. Barker, E. L., Kimmel, H. L., and Blakely, R. D. (1994) *Mol. Pharmacol. 46*, 799−807.
15. Giros, B., Wang, Y. M., Suter, S., McLeskey, S. B., Pifl, C., and Caron, M. G. (1994) *J. Biol. Chem. 269*, 15985−15988.
16. Buck, K. J., and Amara, S. G. (1994) *Proc. Natl. Acad. Sci. U.S.A. 91*, 12584−12588.
17. Buck, K. J., and Amara, S. G. (1995) *Mol. Pharmacol. 48*, 1030−1037.
18. Kitayama, S., Shimada, S., Xu, H., Markham, L., Donovan, D. M., and Uhl, G. R. (1992) *Proc. Natl. Acad. Sci. U.S.A. 89*, 7782−7785.
19. Bismuth, Y., Kavanaugh, M. P., and Kanner, B. I. (1997) *J. Biol. Chem. 272*, 16096−16102.
20. Barker, E. L., Perlman, M. A., Adkins, E. M., Houlihan, W. J., Pristupa, Z. B., Niznik, H. B., and Blakely, R. D. (1998) *J. Biol. Chem. 273*, 19459−19468.
21. Barker, E. L., Moore, K. R., Rakhshan, F., and Blakely, R. D. (1999) *J. Neurosci. 19*, 4705−4717.
22. Penado, K. M., Rudnick, G., and Stephan, M. M. (1998) *J. Biol. Chem. 273*, 28098−28106.
23. Chen, J. G., Sachpatzidis, A., and Rudnick, G. (1997) *J. Biol. Chem. 272*, 28321−28327.
24. Vallee, B. L., and Falchuk, K. H. (1993) *Physiol. Rev. 73*, 79−118.
25. Schwabe, J. W., and Klug, A. (1994) *Nat. Struct. Biol. 1*, 345−349.
26. Alberts, I. L., Nadassy, K., and Wodak, S. J. (1998) *Protein Sci. 7*, 1700−1716.
27. Pifl, C., Giros, B., and Caron, M. G. (1993) *J. Neurosci. 13*, 4246−4253.
28. Johansen, T. E., Scholler, M. S., Tolstoy, S., and Schwartz, T. W. (1990) *FEBS Lett. 267*, 289−294.
29. Gether, U., Marray, T., Schwartz, T. W., and Johansen, T. E. (1992) *FEBS Lett. 296*, 241−244.
30. Giros, B., el Mestikawy, S., Godinot, N., Zheng, K., Han, H., Yang-Feng, T., and Caron, M. G. (1992) *Mol. Pharmacol. 42*, 383−390.
31. Ballesteros, J. A., and Weinstein, H. (1995) *Methods Neurosci. 25*, 366−428.
32. Sealfon, S. C., Chi, L., Ebersole, B. J., Rodic, V., Zhang, D., Ballesteros, J. A., and Weinstein, H. (1995) *J. Biol. Chem. 270*, 16683−16688.
33. Fu, D., Ballesteros, J. A., Weinstein, H., Chen, J., and Javitch, J. A. (1996) *Biochemistry 35*, 11278−11285.
34. Almaula, N., Ebersole, B. J., Zhang, D., Weinstein, H., and Sealfon, S. C. (1996) *J. Biol. Chem. 271*, 14672−14675.
35. Almaula, N., Ebersole, B. J., Ballesteros, J. A., Weinstein, H., and Sealfon, S. C. (1996) *Mol. Pharmacol. 50*, 34−42.
36. Javitch, J. A., Ballesteros, J. A., Weinstein, H., and Chen, J. (1998) *Biochemistry 37*, 998−1006.
37. Ballesteros, J., Kitanovic, S., Guarnieri, F., Davies, P., Fromme, B. J., Konvicka, K., Chi, L., Millar, R. P., Davidson, J. S., Weinstein, H., and Sealfon, S. C. (1998) *J. Biol. Chem. 273*, 10445−10453.
38. Ri, Y., Ballesteros, J. A., Abrams, C. K., Oh, S., Verselis, V. K., Weinstein, H., and Bargiello, T. A. (1999) *Biophys. J. 76*, 2887−2898.
39. Kyte, J., and Doolittle, R. F. (1982) *J. Mol. Biol. 157*, 105−132.
40. Overington, J., Donnelly, D., Johnson, M. S., Sali, A., and Blundell, T. L. (1992) *Protein Sci. 1*, 216−226.
41. Elling, C. E., Nielsen, S. M., and Schwartz, T. W. (1995) *Nature 374*, 74−77.
42. Elling, C. E., and Schwartz, T. W. (1996) *EMBO J. 15*, 6213−6219.
43. Regan, L. (1995) *Trends Biochem. Sci. 20*, 280−285.
44. He, M. M., Voss, J., Hubbell, W. L., and Kaback, H. R. (1995) *Biochemistry 34*, 15667−15670.
45. Sheikh, S. P., Vilardarga, J. P., Baranski, T. J., Lichtarge, O., Iiri, T., Meng, E. C., Nissenson, R. A., and Bourne, H. R. (1999) *J. Biol. Chem. 274*, 17033−17041.
46. Sheikh, S. P., Zvyaga, T. A., Lichtarge, O., Sakmar, T. P., and Bourne, H. R. (1996) *Nature 383*, 347−350.
47. Elling, C. E., Thirstrup, K., Holst, B., and Schwartz, T. W. (1999) *Proc. Natl. Acad. Sci. U.S.A. 96*, 12322−12327.
48. Karlin, A., and Akabas, M. H. (1998) *Methods Enzymol. 293*, 123−145.
49. Smicun, Y., Campbell, S. D., Chen, M. A., Gu, H., and Rudnick, G. (1999) *J. Biol. Chem. 274*, 36058−36064.
50. Thayer, M. M., Flaherty, K. M., and McKay, D. B. (1991) *J. Biol. Chem. 266*, 2864−2871.
51. Hakansson, K., Carlsson, M., Svensson, L. A., and Liljas, A. (1992) *J. Mol. Biol. 227*, 1192−1204.

BI0018335